5-1-2020

Analytic Exoplanet Transit Analysis, and Investigation into WASP, Kepler, and Qatar Systems

Colan Gulla
College of the Holy Cross, col97gulla@gmail.com

College of the Holy Cross
Worcester, Massachusetts

The Thesis of **Colan Gulla**

Entitled: **Analytic Exoplanet Transit Analysis, and Investigation into WASP,**

Kepler, and Qatar Systems

is submitted to the office of Scholar Programs in partial fulfillment of the requirements for graduation with College Honors at the College of the Holy Cross, and has been read and approved by the following:

_____
Advisor

_____
First Reader

_____
Second Reader

_____
Director of College Honors

April 27, 2020

COLLEGE OF THE Holy Cross | College Scholars

Table of Contents

I. Abstract

In this paper we analyze exoplanet transit data. First, we discuss an analytical method of assessing the data similar to the one derived in Agol & Mandel, 2002[1]. The time series photometric data for transits used in this paper was downloaded from the NASA Exoplanet Archive. Similar data was also extracted from the Exoplanet Transit Database for analysis. We use a formula for relative flux from Agol & Mandel, 2002[1] to study the specific transit systems of WASP 1b, WASP 12b, Kepler 1, Qatar 1b and TRES-1b. The formula for relative flux is fit to a set of photometric data for each system using the SciPy optimization package in Python.

We first analyze the development of the geometries, and the physical significance of the output parameters from the optimization. We then apply the analytic method to transit systems under the initial simplification that the star is a uniform source of light. After that, we move to a discussion of linear and nonlinear limb darkening and its effect on the light curve fit and the output parameters. To analyze both sets of parameters from the uniform source and limb darkening approximations, we compare the output parameters for each, and we analyze the fit of the curve to the photometric data in each case. These parameters are then compared to published values. We also discuss the inclination angle of the orbital plane, and how it effects the transit data. We conclude with an analysis of the accuracy of each method.

II. Introduction

Investigation into exoplanet transit data is important so that we may look for other solar systems, analyze them, and compare them to our own. One may extract information about a distant solar system using relative flux data, which is collected as an exoplanet passes between the observer and the host star. As the exoplanet “transits” across the face of a host star, it blocks a small percentage of the light. The amount of light blocked is measurable. In this paper we

model this three-dimensional phenomenon as a two-dimensional projection. A number of different attributes of the exoplanet can be determined from this flux difference including the radius of the exoplanet normalized by the stellar radius, the transit time, and other orbital and planetary parameters. If we have a data set that shows two transits, we can measure the orbital period. Before making those calculations, we explain what is happening during the transit with a useful two-dimensional model.

In this report we use a Python code to determine some orbital and planetary parameters. Specifically, we fit the size of the exoplanet, the transit duration, the impact parameter, and eventually a limb darkening coefficient. These parameters will be defined in the subsequent section. In this report we aim to model a time series light curve of the exoplanet's transit following the analytical method developed by Agol & Mandel, 2002[1]. Time series data was downloaded from the NASA Exoplanet Archive, which stores data from TESS, WASP, and Kepler space telescopes, among others. The data extracted from the archive was only data concerning the relative flux of the star. Each data point is a measurement of the relative flux of a host star at a specific point in time as an exoplanet transits its face.

As the exoplanet transits, the general trend of the photometric data set is a U-shaped curve. Before the transit, the data points show total flux, we call this the *No Transit* phase. When the exoplanet begins its transit, we see that the flux drops gradually during an *Ingress* phase. The Ingress phase is when the exoplanet partially eclipses the star on the way *into* its transit. When projected into two dimensions, the Ingress phase is the slope downward of the relative flux, indicating an increasing amount of area, and thus flux, is being blocked by the exoplanet. The U-shaped data trend reaches its lowest value when the exoplanet is in the *Full Transit* phase near the middle of the star. When projected onto two dimensions, the Full Transit phase occurs when

the entire planetary disk is observed to be inside of the stellar disk. The relative flux value in this phase is minimum using the uniform source approximation. Finally, the exoplanet gradually exits the stellar disk during the *Egress* phase. Flux gradually increases from the time when the planetary disk crosses the edge of the planetary disk, until the exoplanet returns to the *No Transit* phase. These phases, and how they relate to a light curve will become clearer later on in this report.

III. Definitions

Here we define all the necessary quantities to understand the analysis of transit light curves, and their associated variables. Imagine two opaque disks overlapping as a theoretical model. This is a two-dimensional projection of three-dimensional space, and it will be a helpful technique to make our analysis easier. We define useful variables similar to Agol & Mandel, 2002[1], to describe transit geometries. To model the transit, z is the center-to-center distance between the projections of the star and the exoplanet into two-dimensional space. When the planetary disk is observed to be tangent to the stellar disk as in Figure 1 below, z is the sum of the radii of the star and the exoplanet. The radius of the exoplanet and the radius of the star, henceforth denoted R_p and R_* respectively, are normalized by R_* in each system. The normalized radius of the exoplanet is denoted p, and represents the ratio of R_p to R_*, i.e. $p = \frac{R_p}{R_*}$, and the normalized radius of the star is taken to be 1. The impact parameter b is a measure of how close the transit path is to the equator of the star. These quantities can be seen in Figure 1 below. The inclination angle i is the angle between the plane in which the planet's orbit lies, and a perfectly flat orbit subtracted from 90°. When $i = 90°$, $b = 0$ and the transit path traces the equator of the star. If $b = 1$, then the center of the exoplanet barely grazes the bottom of the star during transit.

It is important to note that the inclination angle and the impact parameter are intrinsically tied, since a relatively large inclination causes the impact parameter to be relatively large. The relationship between these two variables will be investigated further in subsequent sections of this report.

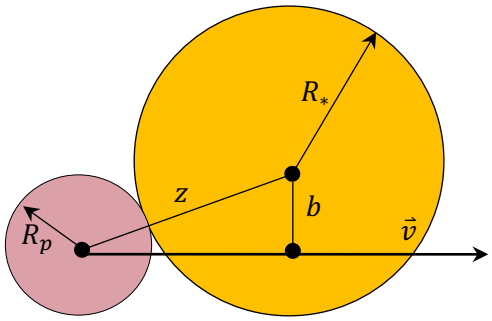

Figure 1: This figure depicts z, the center-to-center distance between the planetary and stellar disks, R_*, the radius of the star, R_p, the radius of the planet, and b, the impact parameter. $\vec{v}$ is the velocity vector of the exoplanet.

The duration of the transit is the time that elapses between when the planetary disk is tangent to the stellar disk the first time, a moment before the Ingress phase, until the instant the planetary disk is tangent to the stellar disk at the end of the Egress phase. This parameter is denoted dt. See the figure below as a reference.

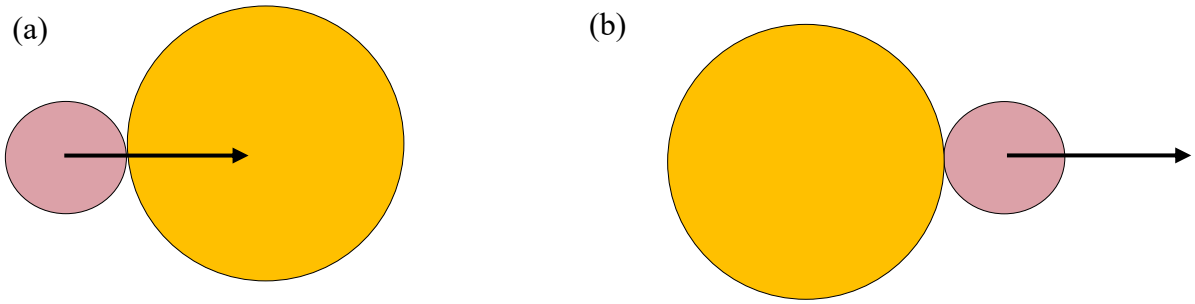

Figure 2: The transit duration dt is the time elapsed from (a) to (b) above.

The final parameter used in our curve fit is t_m, which is the time when the planet is at the middle of its transit. The parameter t_m also marks the time at which $z = b$, when the center-to-center distance between the stellar and planetary disks is at a minimum.

Another useful quantity used throughout this paper is the semimajor axis a, of a planet's orbit. This is the distance from the center of its elliptical orbital path to the center of the planet along the semimajor axis of its orbit. In this paper we can approximate the orbit of the planet to be perfectly circular. This means that a is the orbital radius from the center of the star to the center of the planet at any point in the orbit. We can then approximate the eccentricity, e, of any elliptical orbit to be zero. We will use this definition of a, the orbital radius, when we investigate how the inclination angle effects transit systems.

IV. Uniform Source Transit Geometry

It is important to note that since these systems are so far away, we can only observe transit events when the inclination angle of the system is close to 90°. If this was not the case, then the planet would not pass in front of the star at all. This phenomenon is determined by both the radius of the star and the orbital radius of the planet. When the planet orbits close to the star, the inclination angle can deviate slightly from 90° and we may still observe a transit. When $R_* \ll a$, the planet orbits on a path far away from the star, so the inclination angle has to be almost 90° exactly in order to observe a transit. When the inclination is small, in this case where $R_* \ll a$, we can approximate the transit path to be a perfectly straight line across the face of the star. We use this approximation throughout. When the size of the star is comparable to the size of the orbit, the path that the planet takes across the face of the star is likely a curved one, and in general it is relatively longer than a flat approximation used in the same transit system. For almost all systems, we may approximate the transit path to be a straight line as in Figure 3 below.

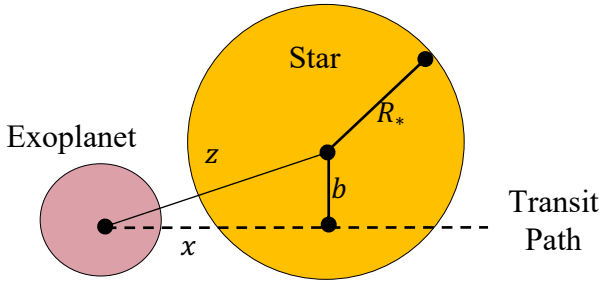

Figure 3: These are the orbital parameters that concern the geometry of the eclipse of two opaque disks. z is the center-to-center distance between the planetary and stellar disks, b is the impact parameter, and x is being defined as the third side of the right triangle with hypotenuse z and altitude b.

We see here that the transit path is modeled as a straight line, even though the impact parameter is non-zero, so it must be the case that the orbital inclination angle is slightly smaller than 90°. We can determine a few properties of interest using simple right triangle trigonometry. We can determine the velocity of the exoplanet in terms of our parameters. When $z = R_p + R_*$, as in Figure 1, we use the Pythagorean theorem to solve for x in Figure 3, and we find that

$$x = \sqrt{(1+p)^2 - b^2}. \quad (1)$$

We see that when the time $t = dt$, the transit duration, the distance the planet travelled is twice the value of x. We are referencing the distance that the center of the exoplanet moves between the events depicted in Figure 2 (a) and (b) above. Solving for the velocity using the general physical equation $x = v * t$, the velocity of the exoplanet in terms of stellar radii per second is:

$$v = \frac{2\sqrt{(1+p)^2 - b^2}}{dt}. \quad (2)$$

Now, we aim to model the orbit of the exoplanet as it transits the star. We use the z parameter as a function of time to model the position of the exoplanet as it transits across the face of the stellar disk. Using the same right triangle as in Figure 3 where $x = v * t$, and again using the Pythagorean Theorem solving for z this time, we see that $z(t) = \sqrt{(v * t)^2 + b^2}$. It is important to note that t in this case is the time measured from the middle of the transit, so $t = t - t_m$. We can now state our model for this section of the planetary orbit by

$$z(t) = \sqrt{v^2(t - t_m)^2 + b^2}. \quad (3)$$

Let us not forget that our goal is to find the flux difference between the total flux of the star, and the flux of the star when the transiting exoplanet is blocking some of the light at every point in time. This analysis defines a piecewise flux equation that separates the transit into four different phases as described briefly in the introduction. Here we will see them in the context of Figure 4 below. The first phase is *No Transit* in Figure 4 (a), when the planetary disk has no overlap with the stellar disk in our model. The second is *Ingress* in Figure 4 (b), where only part of the planetary disk is blocking the stellar disk. *Full Transit* is depicted in Figure 4 (c), and it is when the entirety of the planetary disk is inside the stellar disk. *Egress* is the final phase and it is shown in Figure 4 (d). Egress occurs when the planetary disk is partially overlapping with the stellar disk as the exoplanet exits the face of the star.

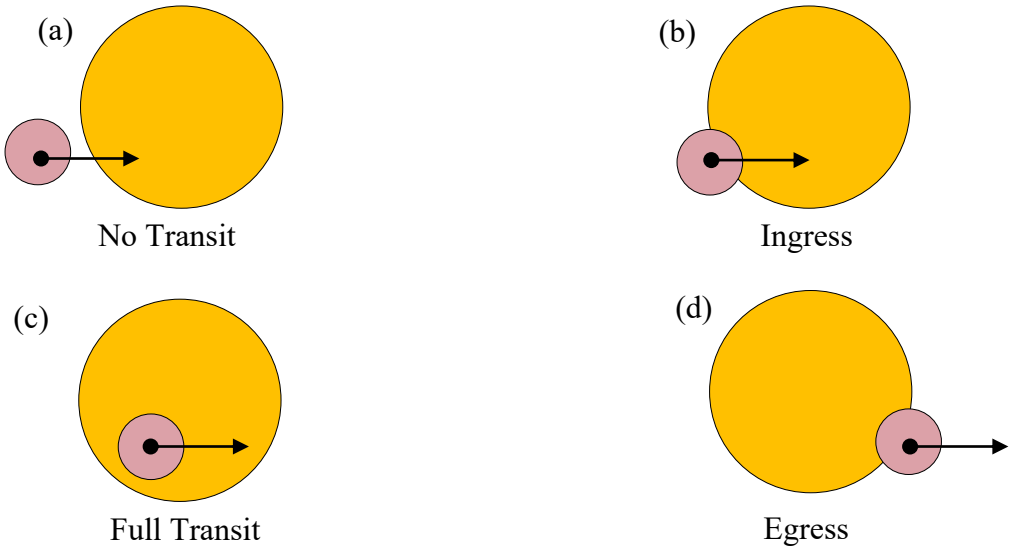

Figure 4: Schematic diagram of the four different phases of a transit as a planet transits its host star.

As we continue to model our relative flux in a similar manner to Agol & Mandel, 2002[1], we need a few additional quantities. We define angles k_0 and k_1 in Figure 5 below.

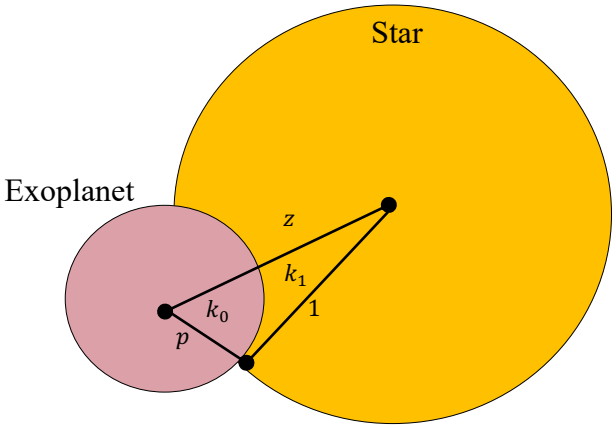

Figure 5: A transiting planet with angles k_0 and k_1 labeled, and the scalene triangle with sides p, z, and 1. We note here that $k_0 = arccos\left(\frac{p^2+z^2-1}{2pz}\right)$ and $k_1 = arccos\left(\frac{1-p^2+z^2}{2z}\right)$ using the law of cosines from this triangle.

During Ingress, the relative flux from the star is proportional to one minus the area of the planetary disk that blocks the star at each moment in time. This is true because we are working under the assumption of uniform brightness. Since we assume the star is uniformly bright across its surface, the amount of brightness blocked by a transiting exoplanet is *directly* proportional to the amount of area blocked by the planet. Thus, we set out to find the area of the segment of the circle that lies over the star as a function of time. The angles defined in Figure 5 will help us to determine this area. The diagram below describes one way to calculate such an area, and it is derived from an area calculation from Agol, et al. 2020[2].

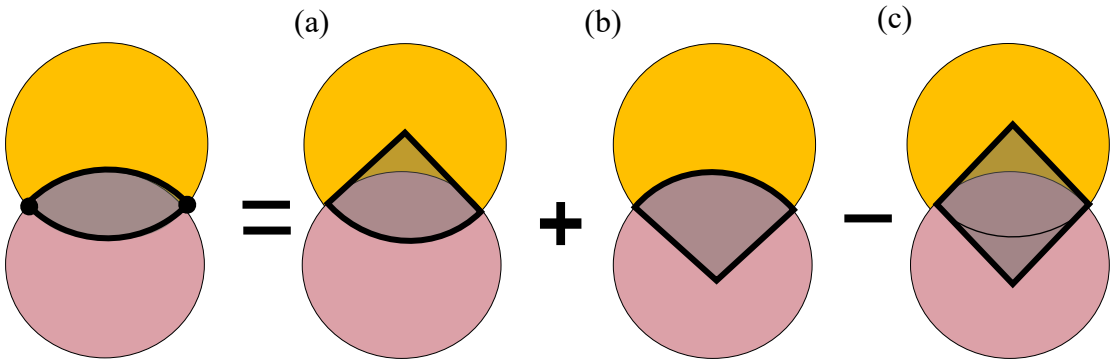

Figure 6: The desired area can be determined using this schematic equation, and the area of each region designated.

The area of the eclipsed region can be calculated by the addition of the two sectors designated in (a) and (b) of Figure 6. Adding these two regions we count the desired area twice, as well as the area of the rest of the kite as shown in Figure 6 (c). Thus, if we subtract the area of the kite, the result is the desired area.

We can compute the area of these regions using a few known area formulas. The area of a sector of a circle is,

$$Area_{sector} = \frac{1}{2}r^2\theta, \tag{4}$$

where θ is the central angle of the sector in radians. The area of a kite can be computed by doubling Heron's formula for area of a triangle when three sides are determined, as shown below.

$$Area_{kite} = \frac{1}{2}\sqrt{(A+B+C)(C-(A-B))(C+(A-B))(A+(B-C))}. \tag{5}$$

where in our case $A = 1$, $B = p$, and $C = z$. Plugging in and solving, we see that the changing area of this transit during the Ingress and Egress phases is

$$\Delta(t) = \left(p^2k_0 + k_1 - \sqrt{\frac{4z^2-(1+z^2-p^2)^2}{4}}\right). \tag{6}$$

Ingress and Egress phases occur when the center-to-center distance between the stellar and planetary disks is between the difference between the radii of the two, and their sum. Represented in terms of our parameters, these phases occur when

$$|1-p| < z \leq 1+p. \tag{7}$$

Let us discuss this calculation further in terms of the four phases of transit described above in Figure 4. During the No Transit phase, we should detect no light blocked, thus our relative flux equation should return value 1. This value designates the full area of the stellar disk normalized by its own area, π. The No Transit phase applies whenever the sum of the center to

center distance between the star and the exoplanet is greater than the sum of the radii of the two. Mathematically, this occurs when

$$z > 1 + p. \tag{8}$$

During the Full Transit phase, we should expect the amount of light blocked to be proportional to the area of the face of the exoplanet as it is projected onto two-dimensional space. This is the area of a circle as usual and will return the value πp^2. Again, we normalize this by the area of the stellar disk to find the relative flux during this phase to be simply p^2. The Full Transit phase applies whenever the center to center distance of the star and the planet is smaller than the difference of the two radii. Mathematically, we have

$$z \leq 1 - p\ . \tag{9}$$

We can at last define the piecewise function that defines the changing area of the star as a planet transits across its uniformly bright face. The function used to fit the parameters is $F(t)$, and it denotes the relative flux of the stellar disk. We define Equation 10, $A(t)$ as the amount of flux blocked by the exoplanet from the uniformly bright star. Mathematically, we write the equation as follows in three different parts:

$A(t) = \frac{1}{\pi}\Delta(t), |1 - p| < z \leq 1 + p$

$A(t) = 0 \qquad z > 1 + p$

$A(t) = p^2, \qquad z \leq 1 - p$

Notice that the area in each phase is normalized by π, the area of the stellar disk. We define $F(t)$, the equation used in our code as

$$F(t) = 1 - A(t). \tag{11}$$

V. Uniform Source Geometry Code

A code was developed that uses the piecewise function $F(t)$. The function describes the amount of light detected from a star as an exoplanet transits the stellar disk. This code operates under the approximation that the star is uniformly bright everywhere on its surface. The code developed reads time series data made available by the NASA Exoplanet Archive from various telescopes. Specifically, we will examine planets detected during the Wide-Angle Search for Planets (WASP) mission, a planet observed during the Kepler mission, a planet observed during the Trans-Atlantic Exoplanet Survey (TRES) and a planet observed during the Qatar Exoplanet Survey (QES). We will begin our examination with a planet called WASP 1b. We calculate using this code, the best fit of the parameters p, the ratio of planet to star radii, dt, the duration of the transit, t_m, the time at which the star was at mid transit when $z = b$, and the impact parameter b. These parameters were fit to the time series data using the SciPy optimization package in Python and compared to other published sources which have computed the same parameters. We are interested specifically in the values for p, dt, and b.

VI. Uniform Source Data and Curve Fits

The figure below shows the best fit model for each of four systems laid over the photometric data from the NASA Exoplanet Archive. Each system was modeled as a uniform source of light.

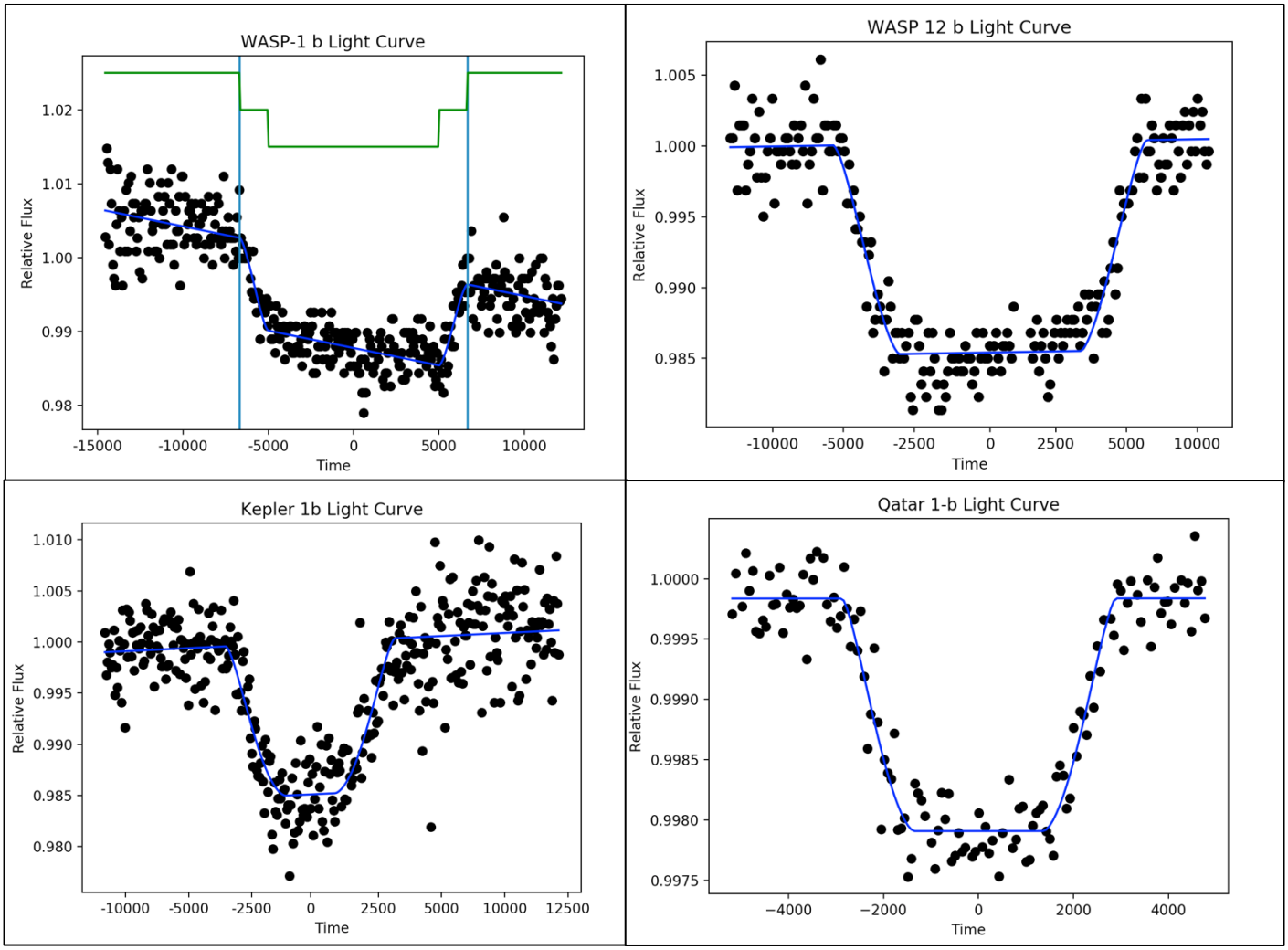

Figure 7: Photometric data of WASP 1b, WASP 12b, Kepler 1b, and Qatar 1b with an overlaid best fit curve. Each has relative flux on the vertical axis, and time elapsed on the horizontal axis. These curves were determined using a least-squares fitting program in Python under the assumption of uniform brightness over the stellar disk.

The results from the best fit model using the least squares fitting function in Python are summarized in Table 1 below. Each system gives three physically significant parameters, p, dt, and b. The normalized planetary radius p and the impact parameter b are distances normalized by the stellar radius, and therefore they must lie between 0 and 1. These three parameters are displayed in Table 1 along with the same parameters found in published papers from investigations carried out by other physicists in the field.

Table I

	WASP 1b	WASP 12b	Kepler 1b	Qatar 1b
Uniform Source Approximation	$p = 0.11 \pm 0.01$ $dt = 13337 \pm 308$ $b = 0.5 \pm 0.1$	$p = 0.12 \pm 0.01$ $dt = 11070 \pm 180$ $b = 0.73 \pm 0.02$	$p = 0.12 \pm 0.01$ $dt = 6685 \pm 212$ $b = 0.85 \pm 0.02$	$p = 0.04 \pm 0.01$ $dt = 5762 \pm 120$ $b = 0.93 \pm 0.01$
Literature	$p = 0.10 \pm 0.01$[3] $dt = 13450 \pm 191$[4] $b = 0.0 \pm 0.1$[3] $b = 0.4 \pm 0.4$[5]	$p = 0.12 \pm 0.01$[6] $dt = 10946 \pm 26$[6] $b = 0.34 \pm 0.01$[6]	$p = 0.13 \pm 0.01$[10] $dt = 6440 \pm 27$[12] $b = 0.84 \pm 0.01$[11]	$p = 0.15 \pm 0.01$[7] $dt = 5980 \pm 29$[8] $b = 0.70 \pm 0.02$[9]

Table 1: The results of the uniform source parameter fits using a least-squares fit in Python for each of 4 systems

As you can see from the plots in Figure 7 above, the general trend of each data set is that when the planet is in the No Transit phase, the relative flux has an approximate value of 1. Once the planet begins the ingress phase a small percentage of the light is blocked, which can be observed as the dip in the relative flux value. After Ingress, the planet is in the Full Transit phase, where the entire planetary disk eclipses a portion of the stellar disk. Full Transit is observed as the section of the data points where the relative flux value flattens, after the first drop in relative flux. The next phase is Egress, which can be observed where the relative flux value increases close to its original value. The exoplanet is in Egress from the time the data trend is upward until it returns to a relatively constant value near 1 once again.

WASP 1 was the first star discovered by a ground-based telescope called Wide Angle Search for Planets. According to the NASA Exoplanet Archive, the WASP 1 star is more massive than the sun, satisfying $M_* = 1.24 M_{sun}$, where M_* is the mass of the star, and M_{sun} is the mass of the sun. It also is slightly larger than the sun, satisfying $R_* = 1.24 R_{sun}$ where R_* is the radius of the star and R_{sun} is the radius of the sun. WASP 1 is about $297\ parsecs$ (pc) away

from Earth. According to Maciejewski, et al. 2014[3], the temperature of WASP 1 is $T = 6252 \pm 45\ K$.

Observe the WASP 1b panel in Figure 7 above. The green line plotted above the data separates the pieces of the function, and the two vertical lines mark the start and finish of the transit. The reason the data does not return to its full original value is because of the change in the airmass through which the telescope that collects the data has to make observations. An object whose light rays have to pass through more atmosphere to a ground-based telescope appears dimmer due to the effects of scattering. Therefore, as the Earth rotates, the stars observed by a telescope on Earth change position, which causes the airmass between the star and the telescope to be different during the course of the observation of the star. In our code we approximate the airmass to change linearly throughout the observation, so we must add a linear polynomial to the flux equation to adjust for the effect. Although they are not given here, the coefficients for this polynomial are also parameters for the curve fit, so they adjust for each data set. A space-based telescope does not need the same airmass adjustment.

To assess the goodness of fit of the uniform source case for each star, we can look to the literature on each system to compare our output parameters. For WASP 1b, we can see from Table 1 that our value for p is in good agreement with the values from the literature. With one standard deviation error for our value, our calculated value overlaps with the published value. For the transit duration dt we see that if we consider our margin of error, about 308 seconds, our results include the published value of 13450 seconds. Finally, for our calculated impact parameter b we see mixed results from published works. In some papers, we see values right around 0.0, which says that the exoplanet transits nearly through the center, or the equator, of the star. Other papers say the exoplanet transits somewhere around 0.4 stellar radii from the center.

Our value for the impact parameter says the exoplanet transits around 0.5 stellar radii from the center. Since there is a large uncertainty about this value across different observations of the system, we can say that it makes sense for the impact parameter to be somewhere between 0.0 and 0.5. This also makes sense because the exoplanet is relatively small compared to the star, which means an impact parameter anywhere within this range would not make a meaningful difference considering the amount of light being blocked by the exoplanet.

The NASA Exoplanet Archive says that the WASP 12 star is also slightly more massive than the sun, satisfying $M_* = 1.43 M_{sun}$. The star also is considerably larger than the sun, with $R_* = 1.66 R_{sun}$. WASP 12 is also about $432\ pc$ away from Earth. According to Collins, et al. 2017[8], the temperature of WASP 12 is $T = 6360 \pm 130\ K$.

Observe the light curve for WASP 12b in the top right panel of Figure 7. The same curve fit function was used as for WASP 1b, this time using different photometric data. As you can see, fewer observations were made throughout the transit in this case than in WASP 1b. Also, these observations were made in such a way that the airmass was nearly constant throughout the time of observation. This likely has to do with the location of this star in our sky, and the line of observation from the telescope to the system since the observations for WASP 12b were made with the same telescope as the WASP 1b system. We do not discuss this airmass phenomenon further in the paper.

Now we will analyze the output parameters for WASP 12b under the uniform source approximation. We can see that our value for p is in good agreement with the value from the literature. For the transit duration, we see from Table 1 that the published value lies within the margin of error in our calculated value, thus we are in agreement on the duration of the transit. However, we differ in our calculation of the impact parameter. Our calculated value is about 0.4

different from the published value. As I mentioned before for WASP 1b, this is likely due to the relative size of the exoplanet. Since the exoplanet is small, this difference in impact parameters will not make significant difference in the amount of light being blocked. Also, as you will see when we discuss limb darkening, our sum squared residual value for this fit is small, this implies that our calculated value for the impact parameter is a feasible one.

The Archive also has information about the Kepler 1b star. We find that it is slightly less massive than the sun, with $M_* = 0.91 M_{sun}$, and it is almost the same size as the sun, satisfying $R_* = 1.06 R_{sun}$. Kepler 1 is also about $186\ pc$ away from Earth. According to Stassun, et al. 2017[19], the temperature of Kepler 1 is $T = 5850 \pm 50\ K$. An alternate name for this exoplanet is TRES 2b, when it was observed by this telescope.

The output parameters for the Kepler 1b system nearly match the literature for each parameter. We calculated p, the relative planetary radius to be about 0.12. This value is the same as the published value even considering the standard error of each. Our calculation of the transit duration also includes the published value within its margin of error. Finally, the published impact parameter for the system was inside the margin of error of our calculated value. Thus, each parameter is in reasonable agreement with the literature.

Next, we look into some of the specifics of the Qatar 1 star. We see from the Archive that the star is less massive than the sun, satisfying $M_* = 0.84 M_{sun}$, and it is slightly smaller than the sun with $R_* = 0.803 R_{sun}$. Qatar 1 is also about $187\ pc$ away from Earth. According to Collins, et al. 2017[8], the temperature of Qatar 1 is $T = 5013 \pm 90\ K$.

For the purpose of comparison to literature sources, and to have an abundance of examples to compare to the limb darkening case for each, we present the well-studied Qatar 1b system. The main observation to notice here is the fact that the transit depth is shallow. The Full

Transit phase shows that only about 0.2% of the light is blocked by the exoplanet. In general, this shallow transit depth could be attributed to either a partial transit, or a small exoplanet radius compared to the stellar radius. In Table 1 below, we can see that the best fit parameters tell us the planetary radius is only just over 4% of the size of the stellar radius.

The parameters for the Qatar 1b system seem slightly off from the published values. We claim that the normalize planetary radius is about 0.04, while the published value is around 0.15. We also estimate the impact parameter to be about 0.93, while the published value is about 0. 7. Although it may not seem as such, these parameters describe a similar situation. In each case, the exoplanet transits fairly low on the star. In our case, the small exoplanet transits very close to the bottom of the stellar disk due to the large impact parameter. The exoplanet blocks light from as low as 0.97 stellar radii from the center. The published values also describe an exoplanet that transits low on the stellar disk. Since it is a relatively larger exoplanet, the transit occurs even lower on the stellar disk, blocking light from as low as 0.85 stellar radii from the center. Thus, these parameters describe a similar transit occurrence, even though the parameters seem significantly different. We can also see that the transit duration is in relatively good agreement with the literature, although it makes physical sense that it is a bit shorter, given the size of our calculated impact parameter.

VII. The Inclination Angle

To continue our discussion of how the inclination angle of the orbit effects the transit data, and our light curve, we observe Figure 8 below.

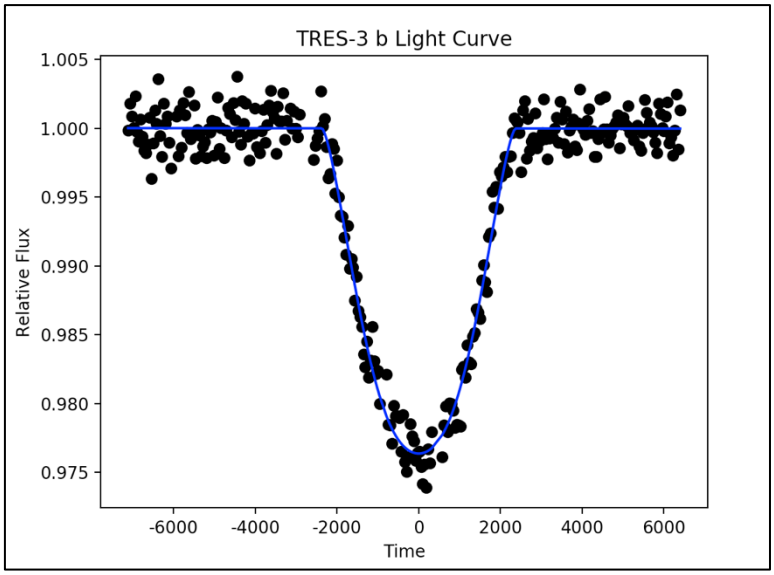

Figure 8: This is the photometric data taken from the NASA exoplanet Archive with the uniform source approximation curve fit for the TRES 3b exoplanet.

The main observation from this plot is the near absence of the full transit phase. We can see there is either no full transit phase—the exoplanet never is entirely inside the face of the star—or the full transit phase is very short. Such a phenomenon is due to the inclination angle of the orbit because according to Sozzetti, et al. 2009[20] the orbital radius of the exoplanet, a, is only about 2 percent of the distance from the Earth to the sun.

The table below summarizes the parameters for this system. We can see again in this case that the transit duration is even shorter than in the Kepler 1b system, and the impact parameter is even larger. It could be the case that the planetary disk is never actually contained in the stellar disk as it is in Figure 4 (c) above, since the normalized radius is relatively larger than the previous two cases. A large relative planetary radius means the planetary disk is large compared to the size of the stellar disk. In this case, the transit depth is somewhat greater than in the

previous two systems, which means a larger portion of the flux from the star was blocked by the exoplanet. The table below summarizes the output parameters for this system.

Table II

Variable	Output	Literature
p	0.16 ± 0.01	0.17 ± 0.01[13]
dt	4737 ± 6	4914 ± 66[14]
b	0.87 ± 0.02	0.83 ± 0.01[15]

Table 2: The parameter summary for the TRES 1b system under the uniform source approximation

As you can see, each parameter is in good agreement with the literature. The value for p explains the relatively large change in flux. The fact that our calculated impact parameter is slightly larger than the published value may be the reason for our shorter calculated transit duration.

The figure below is a diagram which depicts the inclination angle. As you can see, an inclination angle of 90° means that the orbital plane is orthogonal with the zenith. As the inclination decreases, the exoplanet transits lower on the star, giving a larger impact parameter. If the inclination angle is sufficiently small, we will not observe a transit at all, since the exoplanet will not pass between the star and the observer. We can identify the inclination angle as the measure between the axis orthogonal with the orbital plane and the star's zenith. In this paper, we talk about the inclination angle as a measure close to 90°, and i in the figure below is a positive angle measure close to 0°. We can relate the two by subtracting i from 90°. The figure below also illustrates how the impact parameter and the inclination angle are related. If you imagine yourself to be an observer from the right side of the page, and the exoplanet to be in

mid-transit, you can see how an inclination angle somewhat less than 90°, causes an impact parameter somewhat greater than 0. Using simple right triangle trigonometry, one can deduce the relationship between the inclination angle and the impact parameter to be $\frac{b}{a} = \cos i$, where i is defined in Figure 9.

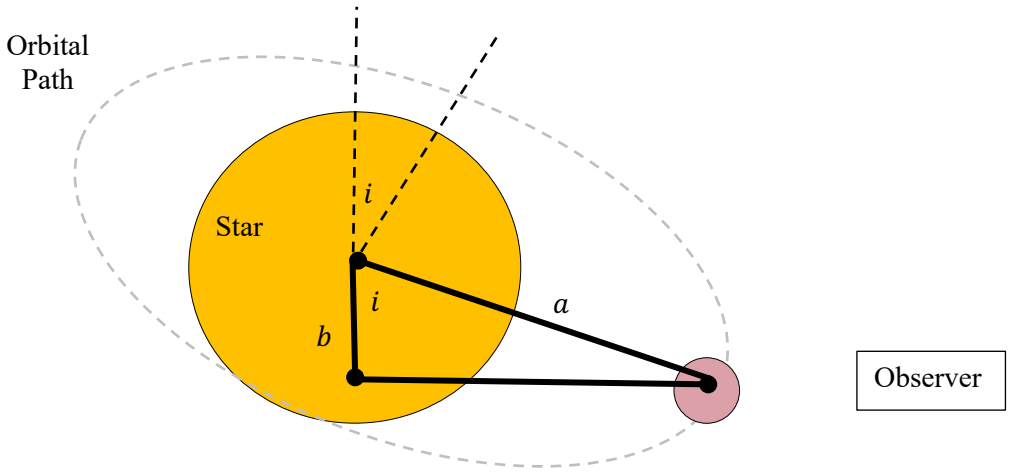

Figure 9: Representation of the inclination angle, and the right triangle geometry used to calculate it.

According to Sozzetti, et al. 2009[20], TRES-3b has a small orbital radius $a = 0.02\ AU$, and the inclination angle is about 81.8°, so an observer sees the exoplanet transit similar to Figure 10 (b) below. All planets we observe using the transit method are somewhere between Figure 10 (a) and (b).

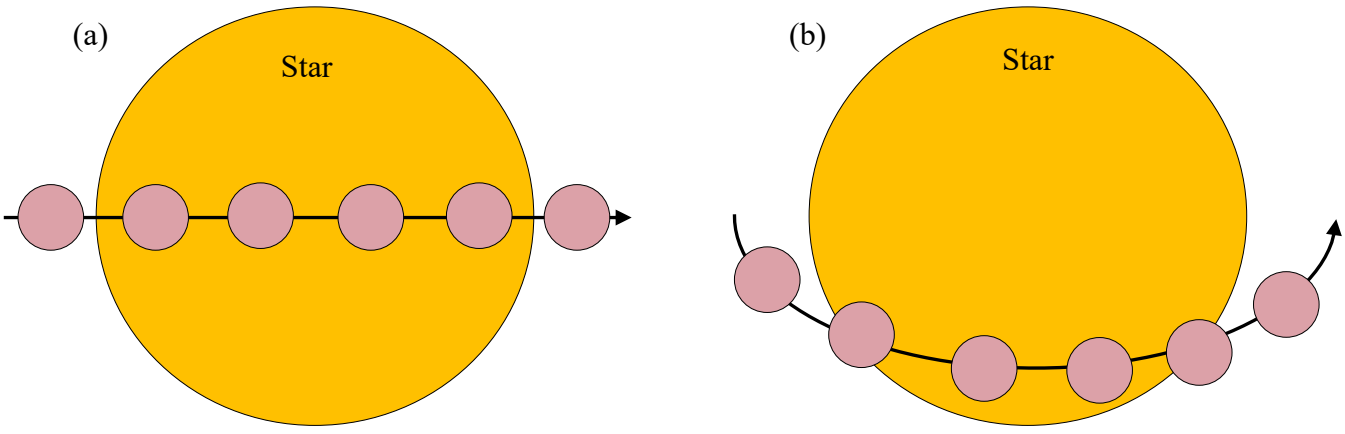

Figure 10: (a) Representation of a transit path with an inclination angle of about 90° (b) Representation of a transit path that has an inclination angle that is somewhat less than 90°, each with planets at different times during its orbit.

As you can see, the transit in (b) above shows a relatively short full transit phase, whereas in (a) the full transit phase is larger for a similar system. In the case where $i \approx 90°$ as shown in Figure 10 (a), the system generally spends more time in full transit than a system which has an inclination angle of somewhat less than 90° because of the geometry of the system. When the orbital radius is considerably larger than the radius of the star, i.e. when $R_* \ll a$, we can approximate the transit path to be a straight line. The difference between Figure 10 (a), and 10 (b) is only apparent when the inclination angle is considerably smaller than 90°, and the orbital radius is relatively small—on the same order as the radius of the star. It is very uncommon to find a system where a is very close to R_*, *and* where the inclination angle is considerably smaller than 90°, so in almost every case the path difference as depicted in Figure 10 (a) and (b) is negligible. Even when the ratio $\frac{a}{R_*} \approx 5$ which is rather small, meaning the orbital radius is only five times the radius of the star, the path difference is still negligible.

VIII. Limb Darkening Geometry

Limb darkening is the phenomena that describes the brightness of the star as a function of the radius, observed relative to the maximum brightness at the center of the stellar disk. The disk of the star is dimmer towards the limbs than at the center. Limb darkening occurs due to the gradient of temperatures through the layers of the star. Since the stars we observe are far from Earth, we cannot directly observe limb darkening effects. They must be inferred in each case because they are unobservable by eye or telescope, and the effects are an intrinsic characteristic to each star. However, we can observe the limb darkening effects in our own sun since it is sufficiently close to us. The figure below from Laurent Corporation shows limb darkening effects in our sun.

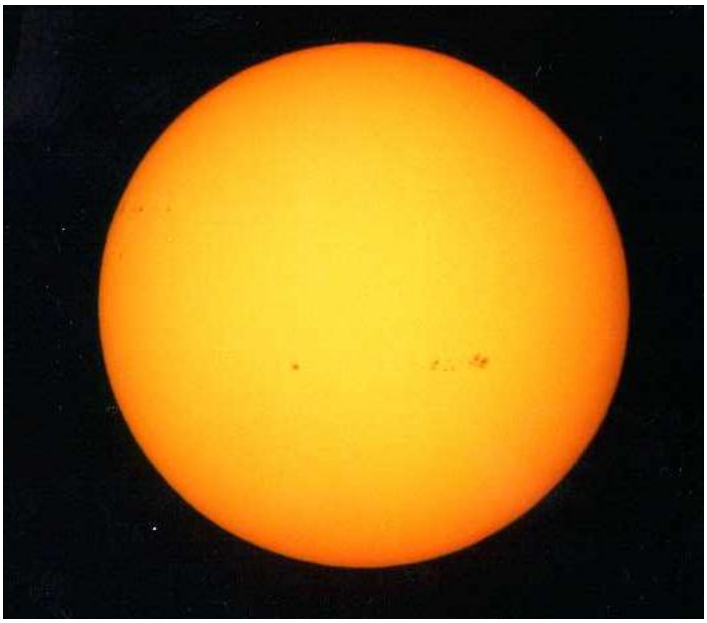

Figure 11: This shows the limb darkening effects of our sun. As you can see, the limbs of the sun are less bright from our perspective than the center of the sun. Image copyright Laurent Corp.

Higher temperatures emit shorter wavelength photons, and lower temperatures emit longer wavelength photons. The photons from a star are emitted from one optical depth within the surface of the star. Because of the geometry of the star, one optical depth at the center of the stellar disk penetrates through to a deeper layer of the star than one optical depth near the limb, therefore we see shorter wavelength, thus brighter, photons emanating from the center of the stellar disk. Figure 12 below shows the geometry of limb darkening.

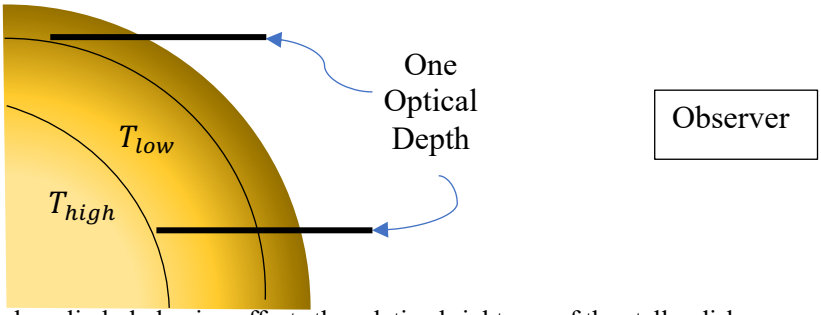

Figure 12: This figure shows how limb darkening effects the relative brightness of the stellar disk.

The analytic function for relative flux detected changes when we consider limb darkening effects. During the Ingress and Egress phases, a transiting exoplanet will block relatively less light than when we consider the stellar disk to be a uniform source of light. This means the brightness blocked by the planetary disk may be different for each point in time. Even when the exoplanet is in Full Transit, the planetary disk could be blocking different amounts of light at each distinct point in time. To tackle this scenario, we can simplify our analysis slightly by assuming that the light being blocked by the planetary disk at any single point in time is uniform. This means there is no gradient of brightness under the planetary disk at any one time. The simplification limits our analysis to exoplanets with a normalized radius of $R_p \approx 0.1$[1]. If the exoplanet is small enough, the gradient of brightness blocked by the planetary disk at any one time is approximately uniform.

Since we use this approximation, we can also modify our calculation for the amount of light blocked. Consider the ingress phase for a small exoplanet relative to its host star. We approximate the area blocked by the exoplanet to be the *segment* of a circle, and not a more rounded shape as in Figure 6. Because the stellar disk is much larger than the planetary disk, the rim of the stellar disk can be treated as a straight line. See the figure below for the geometry.

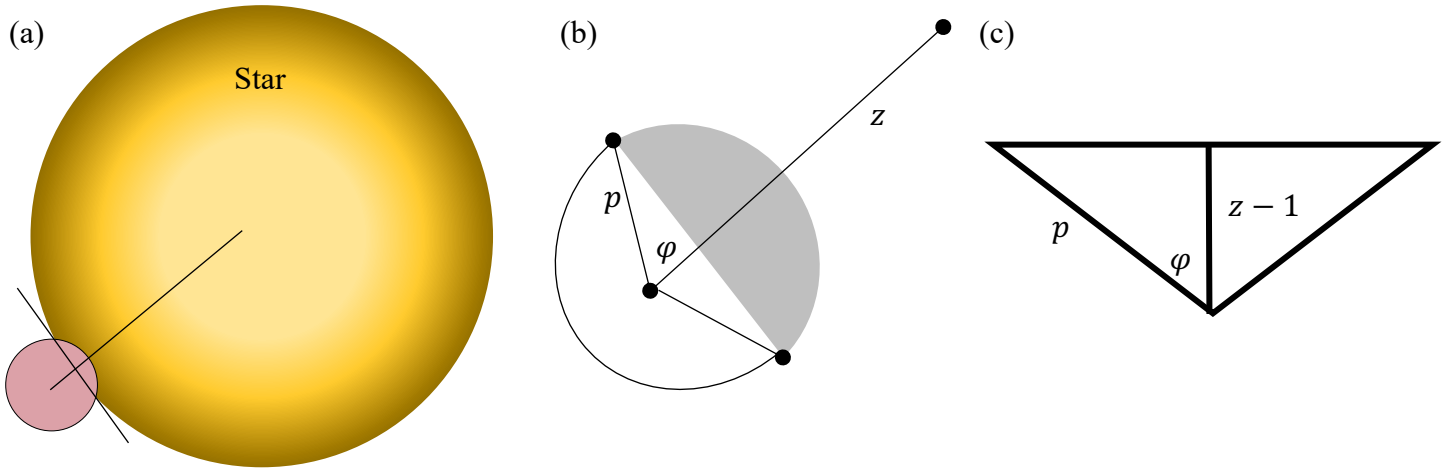

Figure 13: (a) Represents the approximation to the area blocked by the exoplanet as the segment of a circle. (b) is an enlarged version of the exoplanet to show the geometry in detail, where the portion overlapping the stellar disk is shaded grey. (c) is the triangle in part (b) enlarged to show more detail.

As you can see from Figure 13 (a), we approximate the area blocked to be a segment of a circle. For a circle with central angle 2φ, the area of the segment is the area of the sector, when you subtract out the two right triangles in Figure 13 (c). Figure 14 below depicts the geometry.

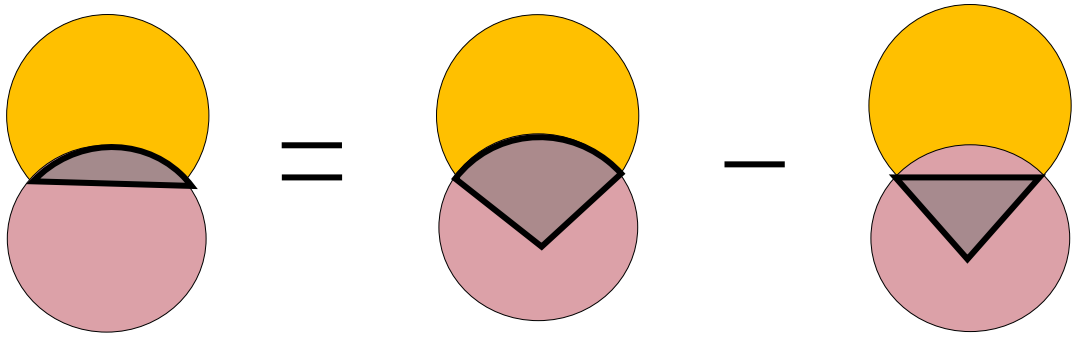

Figure 14: Depicts the geometry of the amount of light blocked by a relatively small exoplanet. Since the stellar disk is much larger than the planetary disk, the system can be approximated by a circle eclipsing a straight line.

The area of the segment is thus;

$$A_{segment} = A_{sector} - A_{triangle}. \tag{12}$$

The central angle in Figure 13 (b) is 2φ. Normally, the area of a sector of a circle with central angle δ and radius r, is $A_{sector} = \frac{1}{2}r^2\delta$, so we can see from Figure 13 (c) that

$$A_{sector} = p^2 arccos\left(\frac{z-1}{p}\right). \tag{13}$$

We also can see from Figure 13 (c) that the area of the two triangles is just the base of the triangle multiplied by its height. Therefore, we have

$$A_{triangle} = (z-1)\sqrt{p^2 - (z-1)^2}, \tag{14}$$

using the Pythagorean theorem to find the base length. Combining Equations 12, 13 and 14, we see that

$$A_{segment} = A_1(t) = p^2 arccos\left(\frac{z-1}{p}\right) - (z-1)\sqrt{p^2-(z-1)^2}. \quad (15)$$

Since we are considering limb darkening, we multiply this area by a brightness coefficient which assumes the exoplanet blocks a uniform source of light at each distinct moment in time.

The area which is calculated by Equation 15 is valid only for Ingress and Egress phases. For the Full Transit phase, we know that the area blocked will be the area of the circular disk of the exoplanet multiplied by the brightness coefficient. For the No Transit phase our function for flux should return a value of 1 for total flux detected from the star. Before we discuss this brightness coefficient, we will define the intensity equation, a necessary prerequisite.

The intensity varies with the radius of the star. We introduce linear limb darkening with the following equation for intensity from Bansal, et al. 2015[16]:

$$I(r) = 1 - \gamma_1(1 - \mu). \quad (16)$$

Here, we have that $\mu = \sqrt{1 - r^2}$ and that γ_1 is the linear limb darkening coefficient. We can say that μ is a measure of distance from the center of the stellar disk in units of stellar radii, and thus $1 - \mu$ is a measure of distance from the limb of the stellar disk. From Equation 16, we can deduce $\gamma_1 < 1$, because the intensity can never be negative. We can generalize Equation 16 for a polynomial of any order with the following sum:

$$I(r) = 1 - \sum_{j=1}^{n} \gamma_j (1 - \mu)^j. \quad (17)$$

In this equation, γ_j are the limb darkening coefficients. Here we are certain that $\sum_{j=1}^{n} \gamma_j < 1$. As we increase j in this sum, the value for γ_j generally decreases. The value for γ_j is generally less significant as j increases. For the purposes of this report, linear limb darkening is sufficient since we will see that the fit of the model is no better when we add more terms to $I(r)$. In the

following plot, we can see an example of the intensity curve for linear and quadratic limb darkening given specific limb darkening coefficients γ_1 and γ_2. The two curves show how the intensity varies with the radius. The two models are most different on the limbs of the star when the radius is large, but you can observe that the two functions are rather similar.

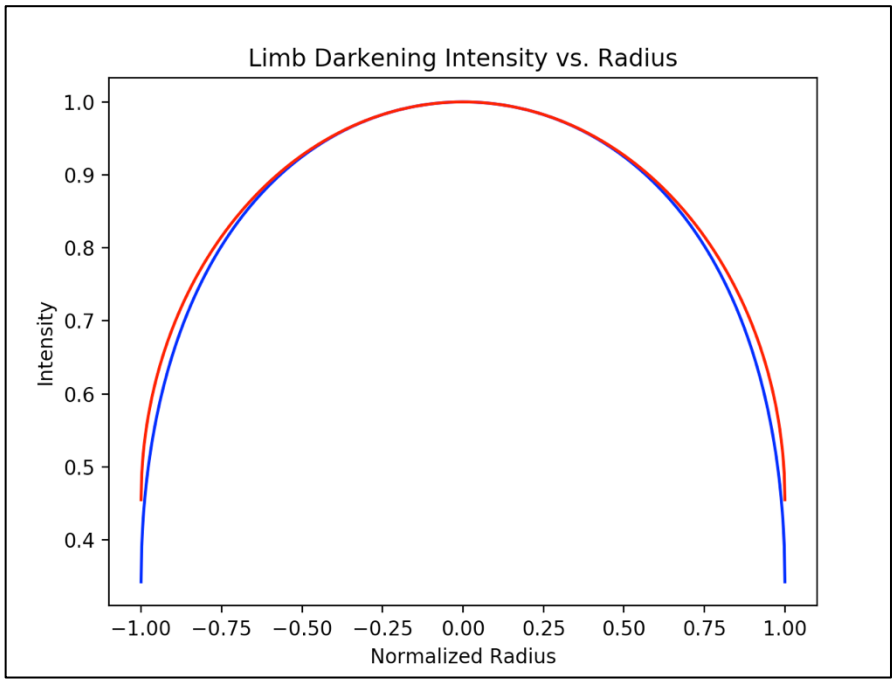

Figure 15: This plot shows both the quadratic and linear limb darkening intensity curves. It shows how intensity varies with the radius of the stellar disk for $\gamma_1 = 0.595$ and $\gamma_2 = 0.1125$, values taken from Bansal, et al. 2015[16], which studies the Qatar 1b system. The linear intensity model is red, and the quadratic intensity model is blue.

In Figure 15 above, we can see the general trend is an increase in intensity as the radius of the stellar disk is closer to zero. This means that the stellar disk is brighter at locations close to the center.

Now we turn to the brightness coefficient, for which we multiply to the area being blocked by the exoplanet for each phase. The brightness coefficient is slightly different for different phases. During Ingress and Egress phases, we have the following brightness coefficient from Agol & Mandel, 2002[1]:

$$L_1(t) = \frac{1}{4\pi\Omega(1-a)} \int_{z-p}^{1} I(r) 2r dr, \tag{18}$$

where r is the radius of the star and the integration variable, $a = (z-p)^2$, $\Omega = \frac{1}{4} - \frac{\gamma_1}{24} - \frac{\gamma_2}{12}$ which are taken from Bansal, et al. 2015[16], and $I(r)$ is the equation for intensity. In the equation for Ω, γ_1 and γ_2 are linear and quadratic limb darkening coefficients, respectively. In the case of linear limb darkening, $\gamma_2 = 0$. For the Full Transit phase, the brightness coefficient changes slightly to the following, using the same definitions for Ω and r above,

$$L_2(t) = \frac{1}{16\pi pz\Omega} \int_{z-p}^{z+p} I(r) 2r dr, \tag{19}$$

when the area of the stellar disk blocked by the exoplanet is

$$A_2(t) = \pi p^2, \tag{20}$$

We can now state the final equation for flux considering limb darkening, $F_1(t)$ to be:

$$\begin{gathered} F_1(t) = 1 - (L_1(t) * A_1(t)) \ |1-p| < z < 1+p \\ F_1(t) = 1 - (L_2(t) * A_2(t)) \ z \leq 1-p, \\ F_1(t) = 1 \qquad z > 1+p \end{gathered} \tag{21}$$

Note that the brightness coefficient also serves to normalize each area by the area of the stellar disk since it divides by a factor of π.

IX. Limb Darkening Code

The code for the uniform source was adapted to account for limb darkening effects. We present the results of the limb darkening fit for each of the star systems in detail. The same parameters were used in the new version of the code, but γ_1 was added as an adjustable parameter for linear limb darkening. The new parameter follows $0 \leq \gamma_1 \leq 1$, and more generally, $0 \leq \gamma_1 \leq \gamma_2 \leq \cdots \leq \gamma_j \leq 1$ if more coefficients were necessary.

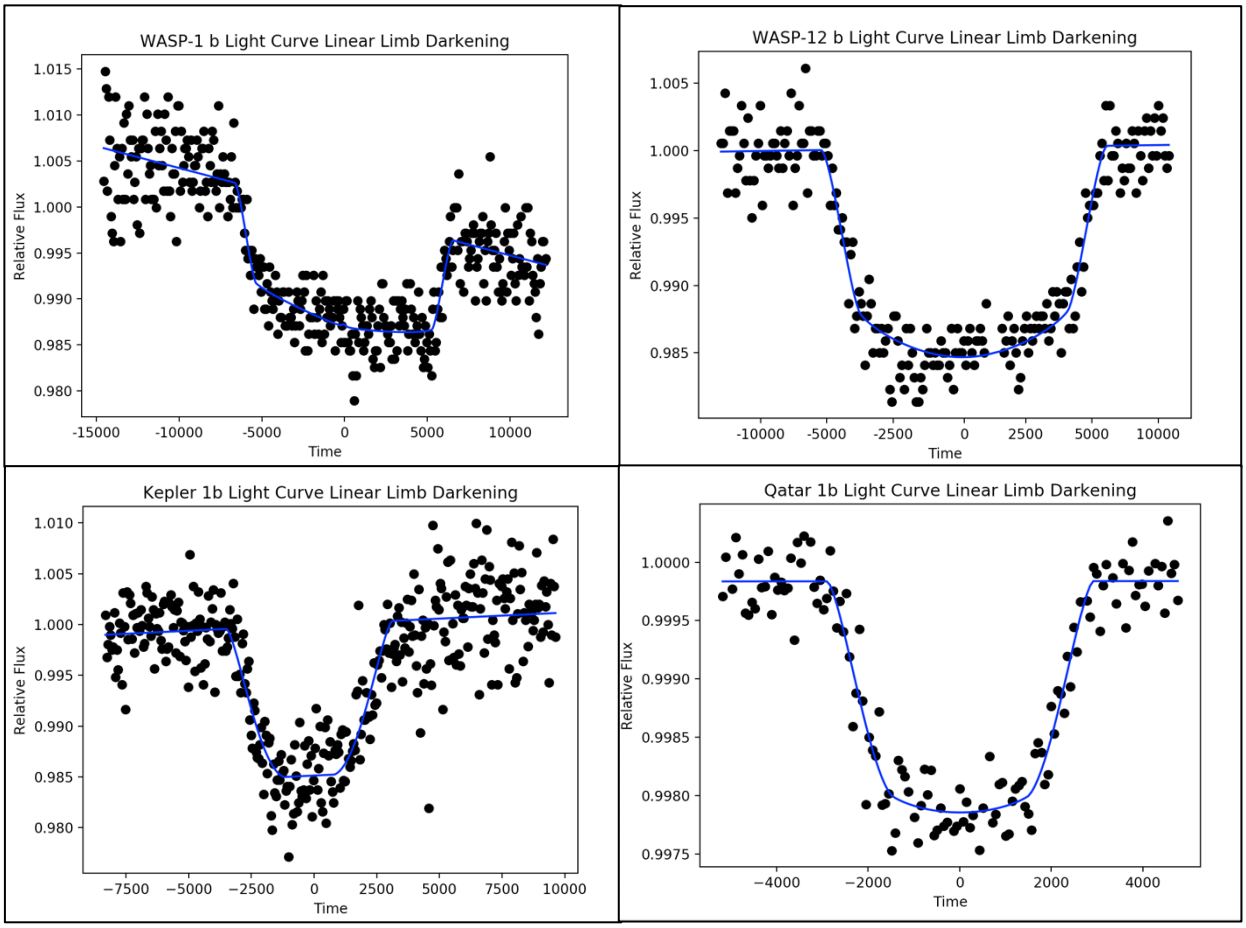

Figure 16: Photometric data of WASP 1b, WASP 12b, Kepler 1b, and Qatar 1b with an overlaid best fit curve. Each has relative flux on the vertical axis, and time elapsed on the horizontal axis. These curves were fit using a least-squares fitting program in Python under the assumption of Linear Limb Darkening.

As one can observe, the Full Transit phase for each of the panels in Figure 16 is most noticeably different from when we treated the stellar disk to be a uniform source. While the transit of the star progresses, we see an increasing amount of the light being blocked as the exoplanet eclipses the disk closer to the center of its transit, than when the exoplanet is closer to the limb.

The limb darkening fit for each system shows the linear limb darkening adjustment, which is also visibly different in the Full Transit phase. Before we reveal statistical data that shows the quality of each fit, observe by eye the difference in fit for each system from Figure 16 above, and

Figure 7. Each curve appears to have a better fit with the limb darkening adjustment than in Figure 7 when we treated the star to be a uniform source of light. We will discuss the quality of the fit in the following section of this report. The results of the best fit parameters from each system in Figure 16 are summarized in Table 3 in the next section.

X. Quality of Fit

We compare the parameters for each limb darkening fit in the table below, to the parameters in the uniform source case outlined in Table 1 above.

Table III

Exoplanet	Uniform Source	Linear Limb Darkening
WASP 1b	$p = 0.11 \pm 0.01$ $dt = 13337 \pm 308$ $b = 0.5 \pm 0.1$ — $\boldsymbol{SSR = 0.003716}$	$p = 0.11 \pm 0.01$ $dt = 13181 \pm 173$ $b = 0.02 \pm 0.11$ $\gamma_1 = 0.3 \pm 0.1$ $\boldsymbol{SSR = 0.003674}$
WASP 12b	$p = 0.12 \pm 0.01$ $dt = 11070 \pm 180$ $b = 0.73 \pm 0.02$ — $\boldsymbol{SSR = 0.000776}$	$p = 0.12 \pm 0.01$ $dt = 10765 \pm 191$ $b = 0.48 \pm 0.102$ $\gamma_1 = 0.47 \pm 0.07$ $\boldsymbol{SSR = 0.000728}$
Kepler 1b	$p = 0.12 \pm 0.01$ $dt = 6685 \pm 212$ $b = 0.85 \pm 0.02$ —	$p = 0.12 \pm 0.04$ $dt = 6618 \pm 298$ $b = 0.85 \pm 0.1$ $\gamma_1 = 0.00 \pm 0.2$

	$\boldsymbol{SSR = 0.00414}$	$\boldsymbol{SSR = 0.00414}$
Qatar 1b	$p = 0.04 \pm 0.01$ $dt = 5762 \pm 120$ $b = 0.93 \pm 0.01$ — $\boldsymbol{SSR = 0.000007}$	$p = 0.05 \pm 0.01$ $dt = 5815 \pm 136$ $b = 0.91 \pm 0.02$ $\gamma_1 = 0.53 \pm 0.3$ $\boldsymbol{SSR = 0.000007}$

Table 3: Comparison of Uniform Source to Linear Limb Darkening Best Fit Parameters, as well as the SSR value for each case.

As you can see, the squared residual value for linear limb darkening model is either smaller, or the same up to the number of digits displayed. In each of WASP 1b and WASP 12b systems, the squared residual value decreased for the linear limb darkening model. We should expect this from our more complex model, since the model depicts a more accurate representation of the stellar surface. As we attempt to make the model more realistic, our curve fit should be more accurate, leading to a smaller sum of squared residuals.

You can also see that the squared residual value only marginally improves with a more refined model of the stellar disk. The reduction in the squared residual value shows that the limb darkening model marginally improves the fit to the data set, and marginally improves the output parameters to more accurately depict the system. Generally, the parameters end up being closer to the literature values in the limb darkening model. Since the literature values also use some polynomial limb darkening model, of course we end up with a value closer to theirs. The literature values selected calculate their parameters using high order polynomial limb darkening. In those high order polynomial limb darkening models, one can adjust the limb darkening coefficients to give a realistic depiction of the stellar surface, which the gives more accurate

parameter outputs. In this report we approximate limb darkening to be linear, so our values should approach the values that use high order limb darkening. We begin to see this improvement with our results for the linear limb darkening approximation. Including polynomial limb darkening gives a genuinely better model for exoplanet transits, and our parameters approach the literature values that use high order polynomial limb darkening.

In the Kepler 1b system the linear limb darkening coefficient is close to zero, so it makes sense that our fit does not improve in this case. As you can see in Table 3, the squared residual value is the same up to the number of digits displayed. For the Qatar 1b system, our fit is already very good for the uniform source case, and the quality of the fit likely improves with the addition of the limb darkening effects. However, this adjustment only contributes a relatively small improvement since the fit is already very good, thus the improvement in the squared residual value is not evident in the number of digits displayed in Table 3 above.

We can also compare the linear limb darkening best fit parameters to the published values in the literature. For WASP 1b, we can see that the value for p stayed more or less the same, still in good agreement with the published value. The transit duration dt for the same system still lies within the uncertainty of the published value, considering its own uncertainty. The impact parameter b changed drastically, but it is still in agreement with the range of acceptable values. This new value for b is in very good agreement with the impact parameter calculated in Maciejewski, et al. 2014[3]. According to Charbonneau, et al. 2007[17], the linear limb darkening coefficient for this system was 0.2, which was in relatively good agreement with our calculated value of 0.3, given our uncertainty of ± 0.1.

The output parameters for WASP 12b under the linear limb darkening approximation stayed more or less the same as in the uniform source case. The values for p and dt stayed in

agreement with the published values as in the uniform source approximation. The impact parameter changed from about 0.73 under the uniform source approximation, to about 0.48 considering limb darkening effects. This new value is considerably closer to the published value of 0.34, and it is even closer taking into account the uncertainty for each. According to Collins, et al. 2017[8], the linear limb darkening coefficient for WASP 12b is about 0.38 ± 0.01, which is close to our calculated value of 0.47 ± 0.07 considering the margin of error for each value. Since our estimates are overall closer to the published values, and our sum of the squared residuals was smaller in this case, we can conclude that the limb darkening was the more accurate model.

For the Kepler 1b system, the limb darkening effects seem to be small. The other parameters each stayed in good agreement with the published values. According to Müller et al 2013[18], the value for the linear limb darkening coefficient was 0.2 ± 0.2. This is close to our calculated value of 0.0 ± 0.2, given their uncertainties.

Finally, for Qatar 1b we see that the parameters change very little from the uniform source approximation fit. The limb darkening effects are significant in this case. Collins, et al. 2017[8] calculates the linear limb darkening term to be 0.58 ± 0.02, which is close to our calculated value of 0.53, when we consider the margin of error of each value.

XI. Conclusion

We can conclude that overall, the limb darkening model was the more accurate one. However, we may be able to improve this model by keeping additional terms in the intensity equation. In theory, keeping more terms should mean a more accurate representation of the limb

darkening effects present on the stellar disk.[†] For the purposes of this paper, linear limb darkening is sufficient, since the sum of the squared residuals is small enough in each case.

We noted earlier in this report that the limb darkening approach uses an approximation to the area in order to simplify our model. This simplification is depicted in Figure 14 above. To improve this approximation further, we could use the area calculated in the uniform source approximation in the limb darkening equation. This would give a more exact calculation of the area. To discuss a final method that would improve the limb darkening approximation even further we note that the current approximation requires the exoplanet to block a uniform amount of brightness, at a single instant in time. Such an approximation is fairly accurate for relatively small exoplanets compared to their host stars, but the approximation is not as accurate for systems with a larger value for the relative planetary radius. Specifically, this approximation requires the exoplanet to be about one-tenth the size of the star. An area of future study can be to derive an equation that allows the exoplanet to be blocking a gradient of light intensities. This would be a more realistic model of a transit occurrence, and it would allow the use of this method with exoplanets that are significantly greater than one-tenth the size of the star. Such an equation would likely improve the curve fit.

We study these exoplanet systems so that we can compare them to our own. For example, Jupiter has a normalized planetary radius of about $p = 0.1$. We can use this photometric data to also investigate the chemical makeup of the atmosphere of the exoplanet. We measure the light that comes from the star and passes through the atmosphere of the exoplanet. The wavelengths of light that are absorbed or scattered by the atoms in the atmosphere are measurable. Observers will notice that the wavelengths of light corresponding to those atoms are missing. The observer

[†] According to Agol et al. 2020[2], after the sixth term is added to make a sextic polynomial, the model "improves imperceptibly."

can determine the atoms that correspond to the missing wavelengths to understand the approximate chemical makeup of the atmosphere. This will be helpful information to determine if life can exist on that exoplanet. This is an additional opportunity for further research with this method, where such data is available. Studying these systems will ultimately help us further understand our own solar system, while pushing our radius of exploration further. While most exoplanets turn out to be uninhabitable "Hot Jupiters," we continue to search for alien Earth-like exoplanets.

XII. References

[1] E. Agol and K. Mandel. "Analytic Light Curves for Planetary Transit Searches," *The Astrophysical Journal Letters*, vol. 580, 2002.

[2] E. Agol, R. Luger, and D. Foreman-Mackey. "Analytic Planetary Transit Light Curves and Derivatives for Stars with Polynomial Limb Darkening," *Draft: GitHub*, January 2020.

[3] G. Maciejewski et al. "Revisiting parameters for the WASP-1 planetary system," *Acta Astronomica*, February 2014.

[4] J. Turner et al. "Ground-based near-UV observations of 15 transiting exoplanets: constraints on their atmospheres and no evidence for asymmetrical transits," *Monthly Notices of the Royal Astronomical Society,* March 2016.

[5] A. Collier Cameron et al. "WASP-1b and WASP-2b: two new transiting exoplanets detected with SuperWASP and SOPHIE" *Monthly Notices of the Royal Astronomical Society,* November 2006.

[6] A. Chakrabarty and S. Sengupta. "Precise Photometric Transit Follow-up Observations of Five Close-in Exoplanets: Update on Their Physical Properties," *The Astronomical Journal*, July 2019.

[7] E. Covino et al. "Observations of the Rossiter-McLaughlin Effect and Characterisation of the Transiting System Qatar-1," *Astronomy & Astrophysics,* March 2013.

[8] K. Collins et al. Transit Timing Variation Measurements of WASP-12b and Qatar-1b: No Evidence of Additional Planets," *The Astronomical Journal,* February 2017.

[9] K. A. Alsubai et al. "Qatar-1b: a hot Jupiter Orbiting a Metal-rich K Dwarf Star," *Monthly Notices of the Royal Astronomical Society,* June 2011.

[10] Y. Ji et al. “An Investigation into Exoplanet Transits and Uncertainties,” *Cornell University Astrophysics Department,* June 2017.

[11] L. Esteves et al. “Changing Phases of Alien Worlds: Probing Atmospheres of *Kepler* Planets with High-Precision Photometry,” *The Astrophysical Journal*, May 2015.

[12] D. Kipping and G. Bakos. “Analysis of Kepler’s Short-Cadence Photometry for TrES-2b,” *The Astrophysical Journal,* May 2011.

[13] G. Torres, J. Winn, and M. Holman. “Improved Parameters for Extrasolar Transiting Planets,” *The Astrophysical Journal,* April 2008.

[14] J. Christiansen et al. “System Parameters, Transit Times, and Secondary Eclipse Constraints of the Exoplanet Systems HAT-P-4, TrES-3, and WASP-3 from the NASA *EPOXI* Mission of Opportunity,” *The Astrophysical Journal*, January 2011.

[15] R. Baluev. “Benchmarking the Power of Amateur Observatories for TTV Exoplanets Detection,” *Monthly Notices of the Royal Astronomical Society,* January 2015.

[16] D. Bansal et al. “Light Curve Analysis for Transit of Exoplanet Qatar-1b,” *Baylor University Department of Astrophysics,* August 2015.

[17] D. Charbonneau et al. “Precise Radius Estimates for the Exoplanets WASP-1b and WASP-2b,” *The Astrophysical Journal*, April 2007.

[18] H. Müller et al. “High-Precision Stellar Limb-Darkening Measurements, A Transit Study of 38 *Kepler* Planetary Candidates,” *Astronomy & Astrophysics*, September 2013.

[19] K. Stassun et al. “Accurate Empirical Radii and Masses of Planets and Their Host Stars with *Gaia* Parallaxes,” *The Astronomical Journal,* March 2017.

[20] A. Sozzetti et al. “A New Spectroscopic and Photometric Analysis of the Transiting Planet Systems TrES-3 and TrES-4,” *The Astrophysical Journal,* February 2009.